Main manuscript for

CARDIAC FIBROBLAST MECHANORESPONSE GUIDES ANISOTROPIC ORGANIZATION OF HIPSC-DERIVED CARDIOMYOCYTES *IN VITRO*

Dylan Mostert[1,2], Leda Klouda[1], Mark C. van Turnhout[1], Nicholas A. Kurniawan[1,2], Carlijn V.C Bouten[1,2]

1 Eindhoven University of Technology, Department of Biomedical Engineering, PO Box 513, 5600 MB Eindhoven, The Netherlands. Tel: +31 (0)402472279

2 Institute for Complex Molecular Systems (ICMS), PO Box 513, 5600 MB Eindhoven, The Netherlands. Tel: +31 (0)402473532

Corresponding author:	Carlijn V.C. Bouten
ORCID:	0000-0003-1035-5094
Postal address:	Eindhoven University of Technology, Department of Biomedical Engineering, PO Box 513, 5600 MB Eindhoven, The Netherlands
Telephone number:	+31 (0)402473006
E-mail address:	c.v.c.bouten@tue.nl

Competing interest statement: The authors declare no competing interests

Keywords: Cardiac mechanosensing, cellular alignment, extracellular matrix patterning, cyclic strain, cardiac co-cultures

This PDF file includes:

Main text
Figures 1 to 7

ABSTRACT

The human myocardium is a mechanically active tissue typified by the anisotropic organization of cells and extracellular matrix (ECM). Upon injury, the composition of the myocardium changes, resulting in disruption of tissue organization and loss of coordinated contraction. Understanding how anisotropic organization in the adult myocardium is shaped and disrupted by environmental cues is thus critical, not only for unravelling the processes taking place during disease progression, but also for developing regenerative strategies to recover tissue function. Here, we decoupled *in vitro* the two major physical cues that are inherent in the myocardium: structural ECM and mechanical strain. We show that patterned ECM proteins control the orientation of the two main cell types in the myocardium: human cardiac fibroblasts (cFBs) and cardiomyocytes (hiPSC-CMs), despite their different mechanosensing machinery. Uniaxial cyclic strain, mimicking the local anisotropic deformation of the myocardium, did not affect hiPSC-CMs orientation. It did however induce a reorientation of cFBs, perpendicular to the strain direction, albeit this strain-avoidance response was overruled in the presence of anisotropic structural cues. These findings reveal that the mechanoresponsiveness of cFBs may be a critical handle in controlling myocardial tissue structure and function. To test this, we co-cultured hiPSC-CMs and cFBs in varying cell ratios to reconstruct normal and pathological myocardium. Contrary to the hiPSC-CM monoculture, the co-cultures adopted an anisotropic organization under uniaxial cyclic strain, regardless of the cell ratio. Together, these results identify the cFBs as a therapeutic target to mechanically restore structural organization of the tissue in cardiac regenerative therapies.

SIGNIFICANCE STATEMENT

Upon cardiac injury, adverse remodeling commonly leads to loss of the anisotropy that is typically found in human adult myocardium. Understanding the role of biophysical cues in shaping and disrupting the anisotropic tissue organization is essential to aid in the progress of cardiac regenerative strategies. Here, we report that the mechanoresponsiveness of cardiomyocytes (hiPSC-CMs) and cardiac fibroblasts (cFBs) differs significantly, resulting in a strain-induced reorganization response for cFBs but not for hiPSC-CMs. In co-culture with varying cell ratios of cFBs and hiPSC-CMs, the co-cultures adopted an anisotropic organization upon cyclic strain administration. Thus, our study proposes the mechanoresponse of cFBs, a cell type often overlooked in cardiac regenerative strategies, as a handle to restore myocardial architecture and function.

Main text

INTRODUCTION

The function of the myocardium is highly dependent on its structural organization of cells and extracellular matrix (ECM). In the healthy human myocardium, cardiomyocytes (CMs) and quiescent cardiac fibroblasts (cFBs) are linearly arranged as dense cellular aggregations surrounded by an anisotropic collagen matrix, enabling electrical and mechanical coupling between CMs and aiding in their synchronous, coordinated contraction [1, 2]. Following cardiac injury, such as ischemic myocardial infarction (MI), billions of CMs die. The ischemia and inflammatory response at the site of injury initiate activation of cFBs towards myofibroblasts. These cells aid in replacing the damaged tissue by synthesizing abundant ECM, but also initiate adverse remodeling of the anisotropic myocardium into disorganized fibrotic tissue. In the continually beating, but mechanically disturbed, myocardium this remodeling is self-maintained, ultimately leading to heart failure [3, 4].

The importance of anisotropic cellular organization for myocardial function has been established with *in vitro* systems. Aligned CMs on two-dimensional (2D) substrates demonstrated improved calcium handling and contractile properties when compared to CM monolayers without orientation [5]. In three-dimensional (3D) cardiac microtissues, aligned CMs and ECM were found to generate a homogeneous coordinated contraction which was not observed in isotropic tissues [6]. Additionally, Tijore et al. showed

that alignment of mesenchymal stem cells (MSCs), induced by gelatin microgrooves stimulated differentiation of the MSCs towards the myocardial lineage [7]. Thus, restoring tissue anisotropy in the damaged myocardium poses a critical step towards functional regeneration. This is particularly relevant because many regenerative strategies have largely focused on replenishing CMs, while the restoration of the myocardial structural organization is often overlooked.

In this study, we investigated how structural and mechanical cues present in the myocardium can guide or disrupt the collective organization of cardiac cells. Specifically, we simulated the fibrous ECM structures and beating of the myocardium, using a 2D *in vitro* approach. CFBs, derived from human fetal epicardial cells, and hiPSC-CMs were cultured on anisotropically or isotropically patterned ECM proteins and subsequently subjected to uniaxial cyclic strain. The results revealed distinct, cell-type-dependent presentation of key mechanosensing factors as well as orientation responses to both guiding cues. To further understand how changes in the cellular composition of the myocardium affect the sensitivity of tissue organization to structural and mechanical cues, we constructed co-cultures of hiPSC-CMs and cFBs with varying cell ratios. Strikingly, we found that the presence of cFBs is sufficient to initiate a strain avoidance response in all co-cultures. These findings can provide new avenues for exploiting mechanical cues to direct cellular organization in the diseased myocardium and aid in cardiac tissue regeneration.

RESULTS

Cellular orientation of cFBs and hiPSC-CMs can be guided by ECM patterning under static conditions

Structurally, the myocardium is a fibrous tissue, implying that cardiac cells receive structural cues from contact with ECM fibers. Similar anisotropic topographical or structural cues from the substrate, such as micropatterns, microfabricated grooves, or collagen fibers, have been shown to guide the orientation of CMs and cFBs – a phenomenon called “contact-guidance” [6, 8–10]. Here, to mimic the local anisotropic structure of the healthy myocardium and allow application of mechanical strain, we created fibronectin (FN) adhesive patterns on deformable polydimethylsiloxane (PDMS) membranes using previously established protocols for microcontact printing (Figure 1) [11]. Three types of patterns were produced: (i) parallel lines with a line width (10 µm, identical to the inter-line spacing, Figure 1A), corresponding to the physiological fiber size of perimysial collagen in the myocardium [12], (ii) crosshatch patterns (orthogonal linear features of 5 µm linewidth and 10 µm spacing, Figure 1B), and (iii) homogeneous FN printed using a homogeneous microstamp as control substrate (Figure 1C). The FN patterns remained intact and well defined throughout the experimental procedures of 48 h of strained or static cell culture.

Both cFBs and hiPSC-CMs showed contact guidance within 24 h of seeding on the printed ECM patterns (Figure 1D – E, G - H). cFBs were aligned in the direction of the parallel lines and consistently displayed an elongated morphology on all FN patterns with an aspect ratio (AR) of 3.5 ± 2.7 on crosshatch patterns and 4.5 ± 2.9 on the parallel patterns. Alignment along the parallel lines was also found for the hiPSC-CMs, although the hiPSC-CMs showed morphological heterogeneity and formed small aggregates on the printed ECM patterns. Such aggregations are often found in CMs upon contraction and involve enhanced cell-cell interactions [11], possibly disturbing the adhesion of hiPSC-CMs to the parallel protein patterns. However, throughout the experiments, the amount of hiPSC-CM on the substrates did not change, suggesting that the vast majority of hiPSC-CMs maintained cell-ECM interactions with the FN patterns. To further analyze the hiPSC-CMs response, we assessed the AR, with hiPSC-CMs demonstrating an AR of 2.1 ± 1.0 on crosshatch patterns and 5.3 ± 1.8 on parallel lines. In general, adult CMs are elongated with an AR of 5, while fetal CMs are typically round. This suggests the immature state of hiPSC-CMs as opposed to adult CMs *in vivo* [13], which is in line with previous reports using human embryonic stem cell-derived cardiomyocytes (hESC-CMs) [14, 15].

Previously, it has been shown that anisotropic ECM induced the alignment of cFBs [14, 16–19], hiPSC-CMs, and neonatal rat CMs [7, 20]. Consistent with these reports, quantification of cell orientation showed a peak in the direction of the parallel FN lines (0º) and random distribution on crosshatch and homogeneous FN for both cFBs and hiPSC-CMs (Figure 1J-L). Notably, a direct comparison between the two cell types on the same, well-defined ECM patterns, revealed that hiPSC-CMs exhibited more pronounced anisotropic orientation than the cFBs (Figure 1J). This is possibly explained by the smaller cell size of the hiPSC-CMs (110 ± 26 µm longitudinal axis) compared to cFBs (242 ± 59 µm longitudinal axis). Indeed, recently, Buskermolen et al. showed that cell size is an important determinant of cell

alignment on ECM patterns and found that the alignment of cardiomyocyte progenitor cells (~100 μm length) occurred at smaller ECM pattern size compared to that of myofibroblasts (~200 μm length) [21]. Taken together, these experiments confirmed that ECM patterning is an effective approach to exploit contact guidance to direct the alignment response of both cFBs and hiPSC-CMs and model organized and disorganized myocardium.

cFBs, but not hiPSC-CMs, show strain avoidance in response to cyclic strain

Mechanically, the myocardium and resident cells experience continuous cyclic mechanical strain due to cardiac beating. Thus, we sought to understand the combined and distinct impacts of ECM structure and cyclic strain on the orientation of cFBs and hiPSC-CMs. The ability of cFBs and hiPSC-CMs to sense and respond to cyclic strain was assessed by analyzing monocultures on the printed ECM patterns that were subsequently subjected to uniaxial cyclic strain at a physiological strain magnitude of 10% and a frequency of 0.5 Hz. In response to such strains, several adherent cell types have been reported to orient perpendicular to the direction of applied cyclic strains – a phenomenon called "strain avoidance" [22–25]. Within 48 hours of cyclic strain on the parallel ECM patterns, both the cFBs and hiPSC-CMs showed a slight disruption of cellular alignment but without a complete strain-avoidance response (Figure 2A, D, G). Quantification of the cell orientation indicates a minor decrease in the fraction of cells oriented at 0°± 5° (contact-guided response) and a lack of alignment in the direction perpendicular to the strain at 90°± 5° (strain avoidance response) (Figure 3A, D). When the starting point was a disorganized cellular organization (on crosshatch ECM patterns and homogeneous FN), the cFBs displayed a clear strain avoidance response, as most cells oriented toward 90º (Figure 2B – C, H – I, blue). This is consistent with the reported response of cFBs on homogeneous ECM [26, 27]. In contrast, uniaxial cyclic strain failed to induce orientation of the hiPSC-CMs away from the direction of the applied dynamic strain (Figure 2E – F, H – I, red). This contrast is further highlighted by the significant increase in the oriented cell fractions at 90°± 5° for cFBs and the lack of change for the hiPSC-CMs (Figure 3E – F). This finding suggests that cFBs and hiPSC-CMs have different intrinsic abilities to sense and respond to cyclic strain.

Mechanosensing machinery differs between cFBs and hiPSC-CMs

Various subcellular structural elements have been identified that enable cells to sense and respond to mechanical cues in their environment [28–30]. Many components of the mechanosensing machinery, such as the actin cytoskeleton and focal adhesions (FAs), have been extensively studied in the context of fibroblast or mesenchymal mechanoresponse [21, 31], but much less in CMs. Previously, it has been observed that contact-guidance cues and cyclic strain evoke opposing effects on the orientations of the actin stress fibers (SFs) orientation and the cell body. Specifically, while the cell bodies follow contact-guidance cues, the SFs can successfully reorganize to orient perpendicular to the direction of strain, suggesting that different mechanisms are involved in the sensing of strain and ECM structure [32]. To investigate the involvements of SFs and FAs in hiPSC-CMs and cFBs in the present study, we developed an image analysis algorithm that can automatically identify single objects (e.g. cells, nuclei, FAs, and SFs) and extract their morphological features. The script ("SFAlab") is available as an open-access MATLAB software and described in the Methods section and Supplementary File S2.

In order to enable singe-cell analysis, we seeded cFBs and hiPSC-CMs on homogeneous FN at a low density, and analyzed the FA and SF distributions, using the SFAlab algorithm (Figure 4). FA formation and alignment has been proposed to play an important role in contact-guided cell response [33]. Our analysis revealed no differences in the size and number of FAs per well between cFBs and hiPSC-CMs (Figure 4E), which is consistent with our observation that both cell types demonstrated contact guidance in response to parallel ECM patterns. On the contrary, hiPSC-CMs exhibited significantly more numerous SFs per cell and more SFs/FA than cFBs (Figure 4F), despite their weaker strain-avoidance response (Figure 2). This may be unexpected, since SFs, together with myosin activity, are known to be key components in strain-avoidance behavior [34, 35], thus a high amount of (active) SFs was anticipated to better facilitate strain-induced reorientation. However, it should be noted that, whereas cFBs express actin SFs, hiPSC-CMs mainly express cortical actin and SFs parallel to the cell membrane, called muscle-specific SFs [36]. Taken together, these findings suggest that the distinct expression and architecture of actin SF impair the mechanoresponsivess of hiPSC-CMs.

Cardiac co-cultures of varying cell ratios reorganize equally in response to uniaxial cyclic strain

Given the stark contrast between the responses of cFBs and hiPSC-CMs to environmental cues, we next asked how their mechanoresponsiveness would dictate the collective cellular organization in myocardial co-cultures. In order to mimic the cellular compositions of normal contractile myocardium and pathological fibrotic myocardium [4, 37], we created co-cultures of hiPSC-CMs and cFBs with either 70:30 (CM-rich) or 30:70 (cFB-rich) cell seeding ratio, respectively. We note that impurities in the hiPSC-CM culture and stronger proliferation of cFBs led to an increased number of non-myocyte cells in the co-culture during the experimental procedure, resulting in co-cultures with 55.3 ± 16.5% α-actinin positive cells for the CM-rich co-cultures and 18.7 ± 9.4% for the cFB-rich co-cultures after 48 hours (Figure S1E). In other words, although the cell composition changed throughout the experimental time period, the number of hiPSC-CMs was always significantly higher in the CM-rich co-culture. Cell viability remained constant between experimental conditions and time points (Figure S1A - D).

Both co-cultures demonstrated cellular alignment on the linear ECM patterns and a random cellular orientation on the crosshatch ECM patterns (Figure 5A, C, E, G), similar to the response of monocultures of cFBs and hiPSC-CMs. Importantly, this allowed us to decouple the effects of cellular composition and organization in modeling the normal and pathological mimicking cell composition. Notably, the effect of contact-guidance was found to be more pronounced for the cFB-rich co-cultures than for the CM-rich co-cultures (Figure 5I), suggesting that the presence of cFBs or the crosstalk between cFBs and hiPSC-CMs can influence the susceptibility of either cell type to contact-guidance cues.

To simulate the mechanical environment in the myocardial niche, where ECM guidance and cyclic strain together influence the organization of cardiac cells, we studied the combinatory effect of uniaxial cyclic strain and (an)isotropic ECM on cFB-rich and CM-rich co-cultures. When uniaxial cyclic strain was applied in the same direction as the anisotropic ECM, both co-cultures lacked a distinct strain-avoidance behavior (Figure 5B, F), even though a small but significant increase was found in the fraction of cells aligned at 90º for the cFB-rich co-culture (Figure 6A, C). These results show that contact-guided cellular organization of cardiac co-cultures cannot be easily disrupted by cyclic strain induced strain-avoidance, at least with the pattern dimensions and strain protocols used in this study.

In order to analyze whether cyclic strain could overpower the disorder that results from disorganized ECM, the cardiac co-cultures were strained after culture on crosshatch patterns. Both the normal (hiPSC-CM-rich) and pathology-mimicking (cFB-rich) co-cultures showed anisotropic reorganization of the cellular monolayers within the 48 hours of dynamic culture (Figure 5D, H, L), suggesting that uniaxial cyclic strain can be used to induce linear organization on disorganized ECM. When assessing the orientation of the hiPSC-CMs and cFBs individually, both cell types showed a strain-induced reorientation response (Figure 7). It is hypothesized that the paracrine factors secreted by the cFBs induce a change in hiPSC-CM mechanoresponse since there is little physical contact between the cFBs and hiPSC-CMs in the cardiac co-cultures. Similarly, the application of uniaxial cyclic strain without contact-guidance cues (i.e. on homogeneous FN) resulted in cell alignment away from the direction of the applied strain for both co-cultures. Surprisingly, no significant difference was observed between the strain-avoidance response of the CM-rich and of the cFB-rich co-cultures (Figure 6D). This was unexpected given that hiPSC-CM monocultures did not show such strain-avoidance response. Therefore, these findings support the notion that cFBs either guide the orientation of hiPSC-CMs when they align in response to strain or that the cFBs influence the responsiveness of hiPSC-CMs to uniaxial cyclic strain. Collectively, these data suggest that the mechanoresponsiveness of cFBs may be critical in determining myocardial tissue structure and function *in vivo*.

DISCUSSION

In our search to develop strategies to regenerate cardiac anisotropy, we aimed to gain fundamental understanding of how biophysical cues from the myocardium contribute to shaping and disrupting anisotropy, in particular by organizing the main cell types in the cardiac wall. To this end, we used a 2D *in vitro* approach of micropatterned ECM protein patterns on deformable substrates, which allows controlled presentation of structural cues and mechanical strains independently and simultaneously to monocultures and co-cultures of cFBs and hiPSC-CMs. We note that the effects of these structural and mechanical cues in particular on the behavior of CMs are relatively unknown.

Analysis of the cells on ECM patterns revealed that structural cues can effectively guide the cellular orientation of cFBs and hiPSC-CMs, resulting in anisotropic organization when cultured on parallel ECM

patterns. Since myocardial tissue mainly consists of parallel collagen I fibers, ECM organization could be a key determinant of cFB and hiPSC-CM organization *in vivo* [38].

Strikingly, distinct responses were observed for cFBs and hiPSC-CMs when ECM patterns and uniaxial cyclic strain were presented simultaneously. We found that hiPSC-CMs were not able to reorient as expected with a strain-avoidance response. This is interesting, because while cyclic strain is often used to enhance cardiomyogenic induction in embryonic stem cells (ESCs) [39] and MSCs [40], only a few studies investigated the effect of cyclic strain on the cellular organization of CMs [41–43]. For cardiomyocyte progenitor cells, it was found that a strain avoidance capacity is developed upon cardiac differentiation [25]. Chun et al. showed that hiPSC-CMs respond differently to different regimens of strain and disease states, demonstrating that static strain promotes the development of sarcomere components whereas cyclic strain increased cell–cell contacts, although no strain-induced reorientation was observed [44]. In contrast to the lack of response by hiPSC-CMs, cFBs demonstrated a strain-avoidance response on parallel patterns and a clear induction of anisotropic organization on the crosshatch patterns. This strain-avoidance response suggests not only that uniaxial cyclic strain can be exploited to restore the anisotropic architecture of the myocardium but also that it can disrupt the anisotropic organization if cFBs dominate the injured area of the myocardium.

These data suggest that cFBs and hiPSC-CMs have different intrinsic abilities to sense and/or respond to cyclic strain. SFs and other actin and actin-binding structures are needed to mediate strain-avoidance behavior [34, 45]. For example, Nava et al. proposed that strain-induced alignment is the consequence of a transient nuclear softening, indicated by a change in conformation of perinuclear actin, the nuclear envelope, and heterochromatins [22]. To explore this, we designed a novel quantification tool to assess the structure and quantity of focal adhesions (FAs) and actin stress fibers (SFs), key players in contact-guidance and strain-avoidance response, respectively. Our results demonstrated that hiPSC-CMs possessed more (active) SFs as opposed to cFBs, whereas no clear differences were found for FA size and distribution. Moreover, whereas cFBs show actin SFs throughout the cell, hiPSC-CMs mainly express cortical and sarcomeric actin. These differences in the mechanosensing machineries between cFBs and hiPSC-CMs may therefore be responsible for the distinct responses of these two cell types to structural and mechanical cues.

To better recapitulate the *in vivo* cellular composition of the myocardium, we next created co-cultures of hiPSC-CMs and cFBs that represent the cellular distribution of the normal (CM-rich) and pathological (cFB-rich) myocardium. The culture of neonatal rat CMs together with cFBs in scaffold-free 3D constructs was found to simulate the *in vivo* cellular distribution and function regarding calcium handling and rhythmic contraction [46], indicating the advantage of using a co-culture to mimic the native cardiac tissue. Co-culture of hiPSC-CMs with cFBs was also reported to result in faster spontaneous contraction and an altered morphology with ultrastructural features comparable to those in the fetal myocardium [47]. A study performed with neonatal rat CMs and cFBs in 3D constructs showed a negative correlation between the amount of cFBs and the beating frequency of the engineered constructs, demonstrating a threshold of around 55% of cFBs, with higher amounts of cFBs negatively affecting the beating frequency of the tissue [6], highlighting the importance of the cell ratio between hiPSC-CMs and cFBs. To date, it is not yet known if changes in the cell ratios of CMs and cFBs during MI change the responsiveness of the myocardium to structural and mechanical cues.

We found that, for both CM-rich and cFB-rich co-cultures, contact-guided alignment on parallel ECM patterns was not disrupted by cyclic strain. Moreover, we demonstrated that cyclic strain could overpower cellular disorganization induced by crosshatch ECM pattern, leading to anisotropic organization of the co-cultures. Interestingly, both co-cultures showed a similar degree of anisotropic organization upon uniaxial cyclic strain, in contrast to what was found for hiPSC-CM monoculture. This strongly suggests a crosstalk between cFBs and hiPSC-CMs where the presence of cFBs influences the mechanoresponsiveness of hiPSC-CMs. This is in line with previous studies that showed that the number and activation state of cFBs modulated the electromechanical functioning of hiPSC-CMs [48–51]. Further studies should be directed to investigating the mechanisms that trigger the strain-induced reorientation response in the CM-cFB co-culture.

Together, our findings indicate that hiPSC-CMs and cFBs, the main cellular components of the myocardium, differentially respond to structural and mechanical cues that typify the myocardial tissue. Importantly, an interplay between the two cell types is necessary for the overall mechanoresponsiveness that leads to anisotropic tissue organization as is expected in healthy, contractile myocardium. Our study proposes the importance of the mechanoresponse of cFBs, a cell type often overlooked in cardiac regenerative strategies, in determining myocardial architecture and function. By exploiting the

mechanoresponsiveness of cFBs to uniaxial cyclic strain, the formation of anisotropic structure in scaffolds and tissue engineering constructs can be promoted, aiding the design of strategies for structural organization of the myocardium. Future studies should indicate how this responsiveness can be exploited in three-dimensional (3D) and *in vivo* heart models as a strategy to regain cardiac anisotropy upon injury.

MATERIALS AND METHODS

Fabrication of micro-patterned deformable substrates: Fibronectin (FN) adhesive patterns were transferred onto deformable PDMS membranes using previously established protocols for microcontact printing [11, 52]. In short, a parallel line pattern (10 µm width, 10 µm gap) and a crosshatch pattern (perpendicular crossing with 5 µm wide lines with 10 µm spacing) were generated on a silicon master wafer by deep reactive-ion etching from a chromium photomask [53]. Microstamps were obtained by molding the silicon master with polydimethylsiloxane (PDMS, Sylgard 184; Dow Corning, Michigan, United States) and curing agent (10:1) and curing the constructs for 20 minutes at 120 °C. Cured PDMS microstamps with the desired features were then peeled off from the master and cleaned and dried with 70% ethanol and compressed air, respectively. In order to print the protein patterns, the microstamps were inked for 1 hour at room temperature with 25 mg/mL rhodamine FN solution (Cytoskeleton Inc., Colorado, United States). Deformable silicone Flexwell membranes (Flexcell inc., Burlington, United States), supported by an underlying printing mold, served as substrates for the microcontact printing. These substrates were first oxidized in an UV/ozone cleaner (PDS UV-ozone cleaner; Novascan, Iowa, United States) for 8 minutes, after which the FN-coated stamps (first dried under compressed air) were gently deposited on the substrates and incubated for 15 minutes at room temperature. Uncoated regions were blocked by immersing the substrates for 5 minutes in 1% Pluronic F-127 (Sigma-Aldrich, Missouri, United States) in PBS. Finally, the membranes were washed three times with phosphate-buffered saline (PBS, Sigma-Aldrich) and stored in PBS at 4°C until further use. A microstamp without any features was used to print homogeneous FN as a control substrate.

Human induced pluripotent stem cell derived cardiomyocyte culture: Human induced pluripotent stem cell derived cardiomyocytes (hiPSC-CMs) were differentiated according to protocol described before [54] and kindly provided by Prof. E. van Rooij (Hubrechts Institute, Utrecht, the Netherlands). hiPSC-CMs were maintained in RPMI 1640 with HEPES and Glutamax (Life Tech, Bleiswijk, the Netherlands) with 2% B27 with insulin (Life Tech) and 1% penicillin/streptomycin (P/S, Sigma-Aldrich). Six days before mechanical stimulation, hiPSC-CMs were plated on the micropatterned deformable substrates in order to allow cryopreservation recovery and spontaneous beating retrieval. Cells were seeded at 50.000 cells/cm^2.

Epicardial-derived cardiac fibroblast culture: Human epicardial-derived cardiac fibroblasts (cFBs) were kindly provided by Prof. M.J.Th.H. Goumans (Leiden University Medical Centre, the Netherlands) and cultured in high-glucose Dulbecco's modified Eagle's medium (Invitrogen, Breda, the Netherlands) supplemented with 10% fetal bovine serum (Greiner Bio-one) and 1% P/S. The cFBs were cultured in flasks coated with 0.1% gelatin from porcine skin in PBS (Sigma-Aldrich) and passaged at 80% confluency. The passage number of the cFBs during mechanical stimulation was between 4 and 8.

Cardiac co-cultures: In order to mimic the contractile and fibrotic cellular composition of the myocardium, hiPSC-CMs were cultured with 30% cFBs (CM-rich) or 70% cFBs (cFB-rich), respectively [4]. The co-cultures were seeded on micropatterned or homogeneous deformable substrates two days before mechanical stimulation at a total density of 50,000 cells/cm^2 to aid recovery of the hiPSC-CMs from cryostorage. cFBs were collected from culture using 0.05% Trypsin/EDTA (Gibco, Eindhoven, the Netherlands) and plated together with the hiPSC-CMs. The co-cultures were maintained in hiPSC-CM medium and incubated at 37°C and 5% CO_2 until analysis. Monocultures of cFBs and hiPSC-CMs were mechanically stimulated as control.

Cyclic straining of mono and co-cultures: The FX-5000™ Tension System (Flexcell inc., Burlington, United States) was used to provide controlled uniaxial cyclic strain to the cardiac cells cultured on the flexible membranes by means of a regulated vacuum pressure that deforms the membrane. The cardiac cultures were seeded one or two days prior to straining to allow for cell adhesion and cellular organization through the printed fibronectin patterns (d_{-1}) and were strained for 48 hours thereafter. Strains of 10% (0.5 Hz, sine wave) were applied to the cardiac cultures, increasing stepwise from day 0 to condition the cells, and reaching 10% strain after 8 hours. On day 0 (before the onset of strain) and after 48 hours (day 2) the samples were collected. Unstrained cardiac mono and co-cultures were used

as control. The cyclic strain applied to the membranes in 2D was validated using image analysis. First, graphite powder was sprayed on top of membranes that were excluded from cell culture and several stretching cycles were recorded by a camera and the applied cyclic strain was measured by the displacement of the graphite pattern with ImageJ.

Quantification of cell orientation: The orientation response of the cardiac cells was determined from triplicates of three independent experiments (n = 9). Cells were incubated with 1 µg/mL calcein AM (Sigma-Aldrich) for 20 min and the orientation of their long axis was analyzed after medium renewal with an inverted microscope (Zeiss Axiovert 200m equipped with an AxioCam HR camera; Zeiss, Sliedrecht, the Netherlands). Only the central parts of the wells, where the strain field was homogeneous as determined using our in-house calibrations, were considered (1 cm^2, 50,000 cells). Cell orientation was quantified with ImageJ, using the Fiji plug-in "directionality", based on Fourier spectrum analysis (Figure S2).

Viability assay: To verify the coexistence of hiPSC-CMs and cFBs in the co-cultures, cell viability was assessed using calcein AM and propidium iodide (Invitrogen) one day after seeding (day 0) and 48 hours after that (day 2). In short, the co-cultures were carefully washed with PBS and incubated with 1 µg/mL calcein AM and 750 nM propidium iodide for 20 minutes at 37º C protected from light. After incubation, the cultures were washed with PBS directly imaged with an inverted fluorescence microscope (Zeiss Axiovert 200m). Images were taken at three random representative spots per condition. Three individual experiments were performed with 2 – 3 replicates (n = 2 – 3) and co-cultures treated with ethanol were used as negative control.

Immunofluorescence staining: The cardiac cells cultured on the Bioflex plates were washed with PBS trice before and after fixation, fixed in 3.7% formaldehyde (Merck, Darmstadt, Germany) for 10 min, and permeabilized for 10 min with 0.5% Triton-X-100 (Merck) in PBS. Two test samples per group were analyzed in three independent experiments (n=6). Non-specific antibody binding was blocked with 1% horse serum (Sigma-Aldrich) in PBS and cells were incubated overnight with primary antibodies in 10% HS in PBS at 4°C. Subsequently, samples were incubated with the primary antibody against FA protein vinculin (V9131, mouse IgG1, 1:400, Sigma Aldrich). Cells were washed six times with PBS for 5 min and incubated with the secondary antibody mouse IgG1 (A21121, Goat, Alexa Fluor 488, 1:200, Millipore) and Alexa Fluor 647 phalloidin (Thermo Fisher Scientific) in PBS for 1 hour. All incubation steps, except primary antibody incubation, were performed at room temperature and all samples were stained for DAPI (1:500, Sigma Aldrich) to visualize the cell nuclei. Afterwards, the membrane samples were mounted with Mowiol (Sigma-Aldrich) on microscopic cover slips and examined with an inverted fluorescence microscope (Zeiss Axiovert 200m).

Quantification of focal adhesions and actin stress fibers: The nuclear, FA and SF morphological features were assessed from DAPI, vinculin, and phalloidin-Atto 647 stained images, respectively. Their properties were analyzed using a novel custom-built script in MATLAB (The Mathworks, Inc, Natick, MA), which is publicly available (http://gitlab.tue.nl/stem/sfalab/-/tree/v0.1-alpha-2u2). Briefly, the images of FAs and SFs were combined and binarized to fit a mask over individual cell bodies. Next, FAs within the masks were analyzed by using grey-scale images of vinculin, which was chosen as a marker for FAs. However, other markers of FAs such as focal adhesion kinase or paxillin could also be used. The FAs were identified using a five-step filtering process to both suppress the signal of soluble vinculin in the cytosol and to enhance the signal from the individual FAs. To do so, the FAs images were processed with top-hat filtering, median filtering, the imsharpen command, thresholding, and a size criterium, respectively. Isolated objects smaller than 0.1 μm^2 were eliminated from the analysis to ensure background noise is eliminated. Quantification of SFs was done by adopting the approach from Elosequi-Artola et al. where FA centroids are tagged, and their locations serve as the starting and ending points for SFs [31](Supplementary File S2). We adapted the approach of Elosegui-Artola et al. so that with our algorithm the fitted curves are completely independent of the accidental orientation of the SFs in the images (of the image frame of reference). With this method, the algorithm can quantify the number and paths of each possible SF. Post-processing of the fitted SF data was used to eliminate values below 0.4 of relative SF intensity by thresholding.

Statistical analysis: Cell orientation data are presented as mean ± standard error of the mean (SEM). Statistical analysis was performed using Wilcoxon matched-pairs signed rank test for non-parametric two group comparison. Significance was assumed when $p < 0.05$. Graphics and statistical analyses were performed with Graphpad Prism software (version 5.04).

ACKNOWLEDGEMENTS

This research was financially supported by the Gravitation Program “Materials Driven Regeneration”, funded by the Netherlands Organization for Scientific Research (024.003.013). dr. N. A. Kurniawan acknowledges financial support from the European Research Council (851960).

REFERENCES

[1] R. H. Anderson, P. F. Niederer, D. Sanchez-Quintana, R. S. Stephenson, and P. Agger, “How are the cardiomyocytes aggregated together within the walls of the left ventricular cone?,” *J. Anat.*, vol. 235, no. 4, pp. 697–705, Oct. 2019.

[2] I. J. LeGrice *et al.*, “Laminar structure of the heart: Ventricular myocyte arrangement and connective tissue architecture in the dog,” *Am. J. Physiol. - Hear. Circ. Physiol.*, vol. 269, no. 2 38-2, 1995.

[3] D. Gabriel-Costa, “The pathophysiology of myocardial infarction-induced heart failure,” *Pathophysiology*. 2018.

[4] A. R. Pinto *et al.*, “Revisiting cardiac cellular composition,” *Circ. Res.*, vol. 118, no. 3, pp. 400–409, 2016.

[5] A. W. Feinberg *et al.*, “Controlling the contractile strength of engineered cardiac muscle by hierarchal tissue architecture,” *Biomaterials*, vol. 33, no. 23, pp. 5732–5741, Aug. 2012.

[6] A. C. C. Van Spreeuwel *et al.*, “The influence of matrix (an)isotropy on cardiomyocyte contraction in engineered cardiac microtissues,” *Integr. Biol. (United Kingdom)*, vol. 6, no. 4, pp. 422–429, 2014.

[7] A. Tijore *et al.* , “Contact guidance for cardiac tissue engineering using 3D bioprinted gelatin patterned hydrogel,” *Biofabrication*, vol. 10, no. 2, Jan. 2018.

[8] E. T. Den Braber, J. E. De Ruijter, L. A. Ginsel, A. F. Von Recum, and J. A. Jansen, “Orientation of ECM protein deposition, fibroblast cytoskeleton, and attachment complex components on silicone microgrooved surfaces,” *J. Biomed. Mater. Res.*, vol. 40, no. 2, pp. 291–300, 1998.

[9] A. W. Feinberg *et al.*, “Controlling the contractile strength of engineered cardiac muscle by hierarchal tissue architecture,” *Biomaterials*, vol. 33, no. 23, pp. 5732–5741, 2012.

[10] J. U. Lind *et al.*, “Cardiac microphysiological devices with flexible thin-film sensors for higher-throughput drug screening,” *Lab Chip*, vol. 17, no. 21, pp. 3692–3703, Nov. 2017.

[11] M. T. Yang, J. Fu, Y. K. Wang, R. A. Desai, and C. S. Chen, “Assaying stem cell mechanobiology on microfabricated elastomeric substrates with geometrically modulated rigidity,” *Nat. Protoc.*, vol. 6, no. 2, pp. 187–213, Feb. 2011.

[12] P. J. Hanley, A. A. Young, I. J. LeGrice, S. G. Edgar, and D. S. Loiselle, “5-Dimensional configuration of perimysial collagen fibres in rat cardiac muscle at resting and extended sarcomere lengths,” *J. Physiol.*, vol. 517, no. 3, pp. 831–837, Jun. 1999.

[13] C. C. Veerman *et al.*, “Chapter 2 Immaturity of stem-cell derived cardiomyocytes: fatal fl aw or soluble problem?” in Inherited Arrhythmia Syndromes, Univerisity of Amsterdam, 2017

[14] A. S. Zhovmer *et al.*, “The role of nonmuscle myosin 2A and 2B in the regulation of mesenchymal cell contact guidance,” *Mol. Biol. Cell*, vol. 30, no. 16, pp. 1961–1973, Jul. 2019.

[15] H. Y. S. Chan, W. Keung, R. A. Li, A. L. Miller, and S. E. Webb, “Morphometric Analysis of Human Embryonic Stem Cell-Derived Ventricular Cardiomyocytes: Determining the Maturation State of a Population by Quantifying Parameters in Individual Cells,” 2015.

[16] S. Al-Haque *et al.*, “Hydrogel Substrate Stiffness and Topography Interact to Induce Contact Guidance in Cardiac Fibroblasts,” *Macromol. Biosci.*, vol. 12, no. 10, pp. 1342–1353, Oct. 2012.

[17] D. Carson *et al.*, “Nanotopography-Induced Structural Anisotropy and Sarcomere Development in Human Cardiomyocytes Derived from Induced Pluripotent Stem Cells,” *ACS Applied Materials and Interfaces*, vol. 8, no. 34. American Chemical Society, pp. 21923–21932, 31-Aug-2016.

[18] M. Khan *et al.*, “Evaluation of Changes in Morphology and Function of Human Induced Pluripotent Stem Cell Derived Cardiomyocytes (HiPSC-CMs) Cultured on an Aligned-Nanofiber Cardiac Patch,” *PLoS One*, vol. 10, no. 5, p. e0126338, May 2015.

[19] J. Macadangdang *et al.*, “Capillary force lithography for cardiac tissue engineering,” *J. Vis. Exp.*, no. 88, Jun. 2014.

[20] H. T. Heidi Au, B. Cui, Z. E. Chu, T. Veres, and M. Radisic, “Cell culture chips for simultaneous application of topographical and electrical cues enhance phenotype of cardiomyocytes,” *Lab Chip*, vol. 9, no. 4, pp. 564–575, 2009.

[21] A. B. C. Buskermolen *et al.*, “Cellular Contact Guidance Emerges from Gap Avoidance,” *Cell Reports Phys. Sci.*, vol. 1, no. 5, p. 100055, May 2020.

[22] M. M. Nava *et al.*, “Heterochromatin-Driven Nuclear Softening Protects the Genome against Mechanical Stress-Induced Damage,” *Cell*, vol. 181, no. 4, pp. 800-817.e22, May 2020.

[23] M. Moretti, A. Prina-Mello, A. J. Reid, V. Barron, and P. J. Prendergast, “Endothelial cell alignment on cyclically-stretched silicone surfaces,” *J. Mater. Sci. Mater. Med.*, vol. 15, no. 10,

pp. 1159–1164, 2004.
[24] C. Huang *et al.*, “Biological effects of cellular stretch on human dermal fibroblasts,” *J. Plast. Reconstr. Aesthetic Surg.*, vol. 66, no. 12, pp. e351–e361, 2013.
[25] A. Mauretti *et al.*, “Cardiomyocyte progenitor cell mechanoresponse unrevealed: Strain avoidance and mechanosome development,” *Integr. Biol. (United Kingdom)*, vol. 8, no. 9, pp. 991–1001, 2016.
[26] G. S. Ugolini *et al.*, “On-chip assessment of human primary cardiac fibroblasts proliferative responses to uniaxial cyclic mechanical strain,” *Biotechnol. Bioeng.*, vol. 113, no. 4, pp. 859–869, Apr. 2016.
[27] N. A. M. Bax *et al.*, “In vivo and in vitro Approaches Reveal Novel Insight Into the Ability of Epicardium-Derived Cells to Create Their Own Extracellular Environment,” *Front. Cardiovasc. Med.*, vol. 6, Jun. 2019.
[28] Y. Chen, L. Ju, M. Rushdi, C. Ge, and C. Zhu, “Receptor-mediated cell mechanosensing,” *Mol. Biol. Cell*, vol. 28, no. 23, pp. 3134–3155, 2017.
[29] D. E. Dostal *et al.*, “Mechanosensing and regulation of cardiac function,” *J. Clin. Exp. Cardiol.*, vol. 5, no. 6, pp. 1–13, 2014.
[30] Z. Jahed, H. Shams, M. Mehrbod, and M. R. K. Mofrad, *Mechanotransduction pathways linking the extracellular matrix to the nucleus*, 1st ed., vol. 310. Elsevier Inc., 2014.
[31] A. Elosegui-Artola *et al.*, “Image analysis for the quantitative comparison of stress fibers and focal adhesions,” *PLoS One*, vol. 9, no. 9, 2014.
[32] W. W. Ahmed *et al.*, “Myoblast morphology and organization on biochemically micro-patterned hydrogel coatings under cyclic mechanical strain,” *Biomaterials*, vol. 31, no. 2, pp. 250–258, Jan. 2010.
[33] A. I. Teixeira, G. A. Abrams, P. J. Bertics, C. J. Murphy, and P. F. Nealey, “Epithelial contact guidance on well-defined micro- and nanostructured substrates,” *J. Cell Sci.*, vol. 116, no. 10, pp. 1881–1892, May 2003.
[34] C. Tamiello *et al.*, “Cellular strain avoidance is mediated by a functional actin cap - observations in an Lmna-deficient cell model,” *J. Cell Sci.*, vol. 130, no. 4, pp. 779–790, Feb. 2017.
[35] C. Tamiello, C. V. C. Bouten, and F. P. T. Baaijens, “Competition between cap and basal actin fiber orientation in cells subjected to contact guidance and cyclic strain,” *Sci. Rep.*, vol. 5, 2015.
[36] A. M. Fenix *et al.*, “Muscle-specific stress fibers give rise to sarcomeres in cardiomyocytes,” *Elife*, vol. 7, 2018.
[37] P. Zhou and W. T. Pu, “Recounting cardiac cellular composition,” *Circulation Research*, vol. 118, no. 3. Lippincott Williams and Wilkins, pp. 368–370, 2016.
[38] M. A. Horn and A. W. Trafford, “Aging and the cardiac collagen matrix: Novel mediators of fibrotic remodelling,” *Journal of Molecular and Cellular Cardiology*, vol. 93. Academic Press, pp. 175–185, 01-Apr-2016.
[39] S. J. Gwak *et al.*, “The effect of cyclic strain on embryonic stem cell-derived cardiomyocytes,” *Biomaterials*, vol. 29, no. 7, pp. 844–856, Mar. 2008.
[40] Y. Huang *et al.*, “Effect of cyclic strain on cardiomyogenic differentiation of rat bone marrow derived mesenchymal stem cells,” *PLoS One*, vol. 7, no. 4, p. 34960, Apr. 2012.
[41] S. J. Gwak *et al.*, “The effect of cyclic strain on embryonic stem cell-derived cardiomyocytes,” *Biomaterials*, vol. 29, no. 7, pp. 844–856, Mar. 2008.
[42] N. Shen *et al.*, “Steps toward Maturation of Embryonic Stem Cell-Derived Cardiomyocytes by Defined Physical Signals,” *Stem Cell Reports*, vol. 9, no. 1, pp. 122–135, Jul. 2017.
[43] A. Shradhanjali, B. D. Riehl, J. S. Lee, L. Ha, and J. Y. Lim, “Enhanced cardiomyogenic induction of mouse pluripotent cells by cyclic mechanical stretch,” *Biochem. Biophys. Res. Commun.*, vol. 488, no. 4, pp. 590–595, Jul. 2017.
[44] Y. W. Chun *et al.*, “Differential responses of induced pluripotent stem cell-derived cardiomyocytes to anisotropic strain depends on disease status,” *J. Biomech.*, vol. 48, no. 14, pp. 3890–3896, Nov. 2015.
[45] C. Tamiello, C. V. C. Bouten, and F. P. T. Baaijens, “Competition between cap and basal actin fiber orientation in cells subjected to contact guidance and cyclic strain,” *Sci. Rep.*, vol. 5, 2015.
[46] B. R. Desroches *et al.*, “Functional scaffold-free 3-D cardiac microtissues: A novel model for the investigation of heart cells,” *Am. J. Physiol. - Hear. Circ. Physiol.*, vol. 302, no. 10, p. H2031, May 2012.
[47] P. Beauchamp *et al.*, “3D Co-culture of hiPSC-Derived Cardiomyocytes With Cardiac Fibroblasts Improves Tissue-Like Features of Cardiac Spheroids,” *Front. Mol. Biosci.*, vol. 7, Feb. 2020.

[48] S. M. Biendarra-Tiegs, D. J. Clemens, F. J. Secreto, and T. J. Nelson, “Human Induced Pluripotent Stem Cell-Derived Non-Cardiomyocytes Modulate Cardiac Electrophysiological Maturation through Connexin 43-Mediated Cell-Cell Interactions,” *Stem Cells Dev.*, vol. 29, no. 2, pp. 75–89, Jan. 2020.
[49] E. Giacomelli *et al.*, “Human-iPSC-Derived Cardiac Stromal Cells Enhance Maturation in 3D Cardiac Microtissues and Reveal Non-cardiomyocyte Contributions to Heart Disease,” *Cell Stem Cell*, vol. 26, no. 6, pp. 862-879.e11, Jun. 2020.
[50] H. Nakanishi *et al.*, “Geometrical patterning and constituent cell heterogeneity facilitate electrical conduction disturbances in a human induced pluripotent stem cell-based platform: An in vitro disease model of atrial arrhythmias,” *Front. Physiol.*, vol. 10, no. JUN, 2019.
[51] C. E. Rupert, T. Y. Kim, B. R. Choi, and K. L. K. Coulombe, “Human Cardiac Fibroblast Number and Activation State Modulate Electromechanical Function of hiPSC-Cardiomyocytes in Engineered Myocardium,” *Stem Cells Int.*, vol. 2020, 2020.
[52] J. L. Wilbur, A. Kumar, H. A. Biebuyck, E. Kim, and G. M. Whitesides, “Microcontact printing of self-assembled monolayers: Applications in microfabrication,” *Nanotechnology*, vol. 7, no. 4, pp. 452–457, Dec. 1996.
[53] I. A. E. W. van Loosdregt *et al.*, “Intrinsic Cell Stress is Independent of Organization in Engineered Cell Sheets,” *Cardiovasc. Eng. Technol.*, vol. 9, no. 2, pp. 181–192, 2018.
[54] S. Bhattacharya *et al.*, “High efficiency differentiation of human pluripotent stem cells to cardiomyocytes and characterization by flow cytometry,” *J. Vis. Exp.*, no. 91, Sep. 2014.

FIGURES

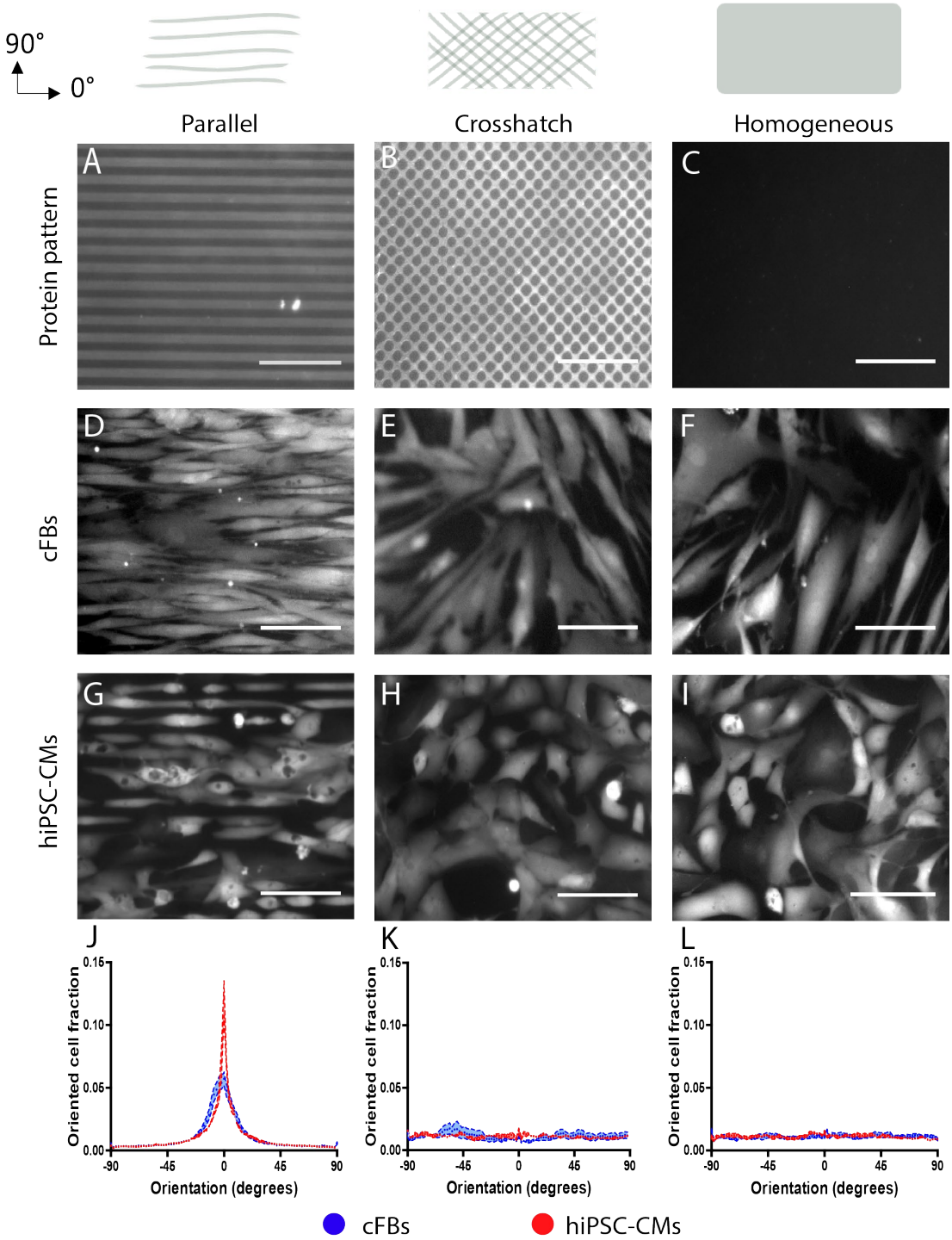

Figure 1: Fibronectin (FN) patterns obtained by micro-contact printing onto deformable PDMS substrates guide organization of cFBs and hiPSC-CMs. A - C) Representative fluorescence images (TRITC-fibronectin) showing anisotropic FN lines, crosshatch FN patterns and homogeneous FN coating. D - I) Representative fluorescence images (calcein AM) of cFBs (D – F) and hiPSC-CMs (G – I) after 24 hours of static cell culture. J – L) Frequency distribution graphs display the cell orientation with respect to the horizontal direction (0º) for cFBs (blue) and hiPSC-CMs (red). Scale bar indicates 100 µm. Results are expressed as mean ± SEM (n = 9 from 3 independent experiments).

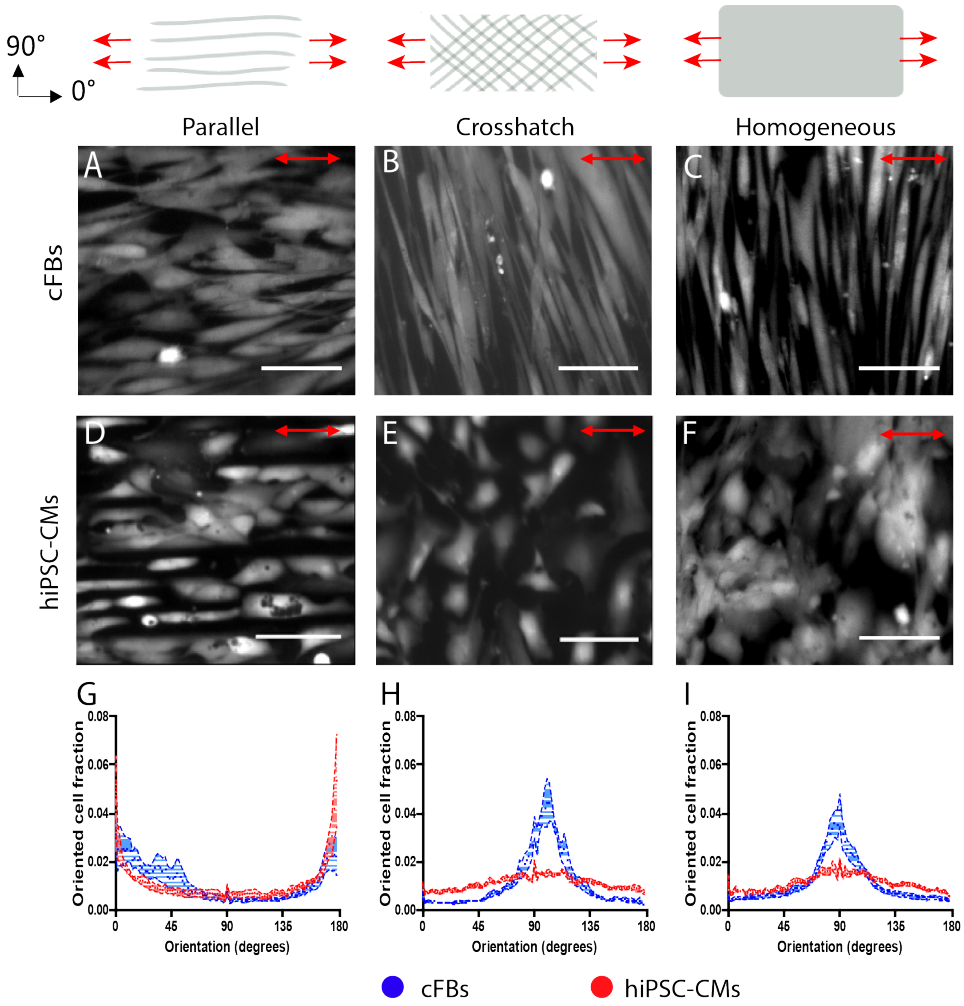

Figure 2: cFBs show a clear strain avoidance response, whereas hiPSC-CMs do not. A - F) Representative fluorescence images (calcein AM) of cFBs and hiPSC-CMs after 48 hours of dynamic culture. The direction of the uniaxial cyclic strain is shown by the arrow. G - I) Frequency distribution graphs comparing the response of cFBs (blue) and hiPSC-CMs (red) display a clear peak at 90º for cFBs on crosshatch and homogeneous ECM while this is not observed for hiPSC-CMs. Scale bar indicates 100 µm. Results are expressed as mean ± SEM (n = 9 from 3 independent experiments).

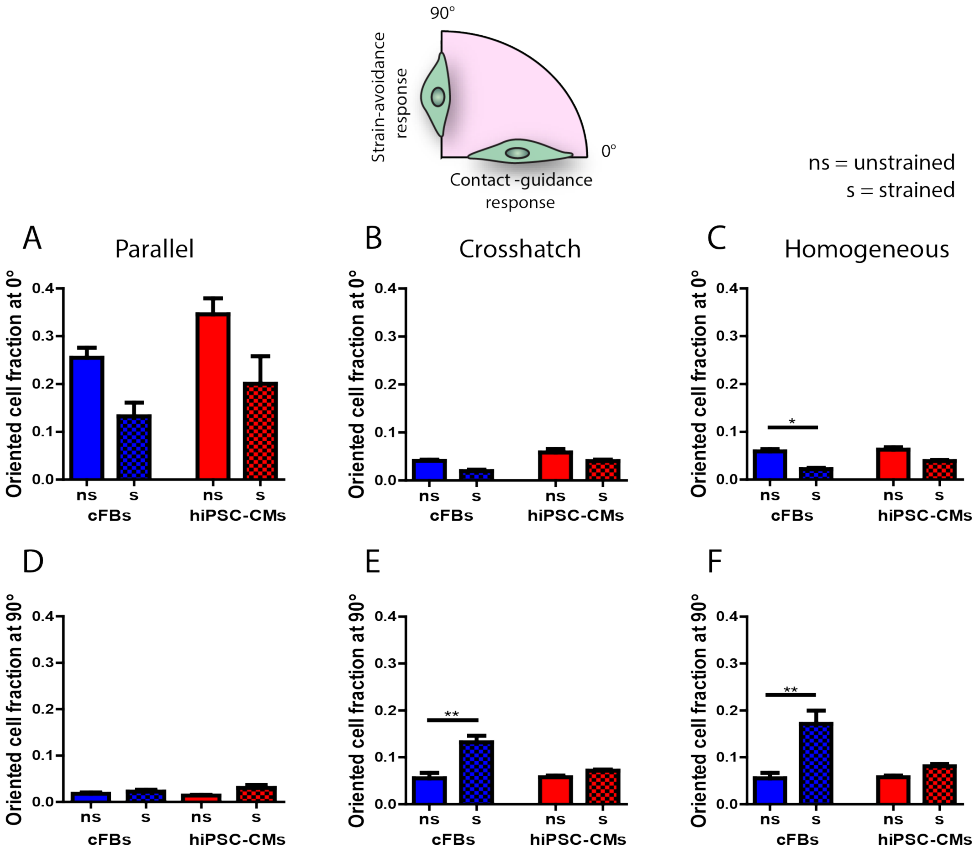

Figure 3: Cyclic strain induces the alignment of cFBs on crosshatch or homogeneous fibronectin. A - F) Oriented cell fractions at 0º ± 5º and 90º ± 5º, showing significant reorganization of the cFBs (blue) upon administration of uniaxial cyclic strain whereas this is not observed for hiPSC-CMs (red). ns = non-strained, s=strained. Scale bar indicates 100 µm. Results are expressed as mean ± SEM (n = 9 from 3 independent experiments); * = P < 0.05; ** = P < 0.01.

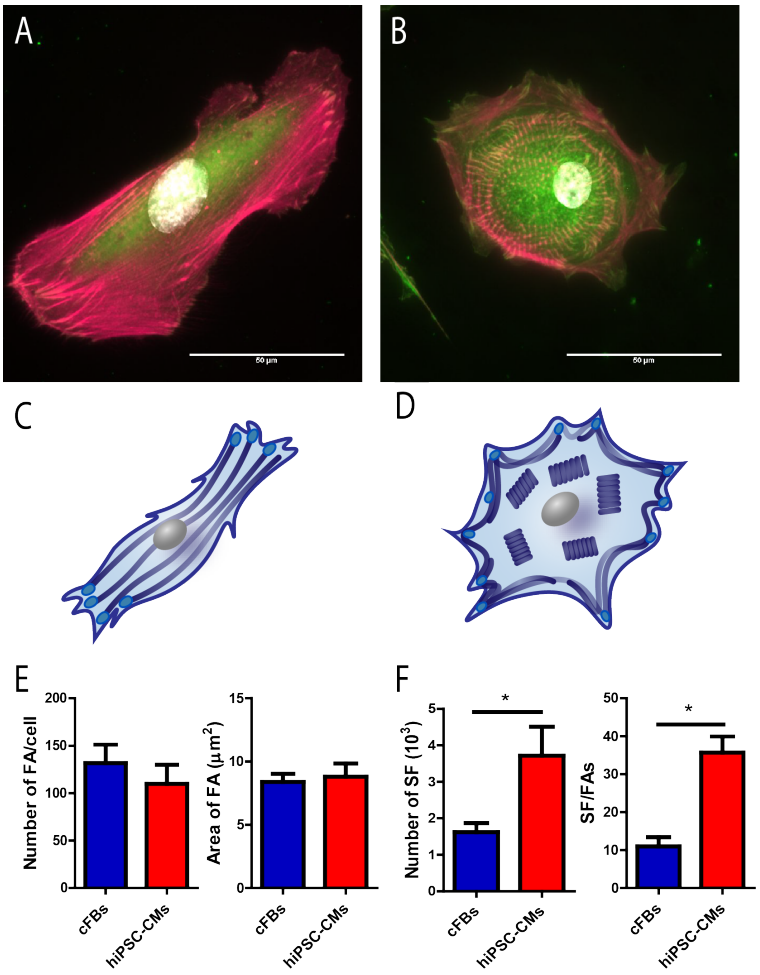

Figure 4: cFBs and hiPSC-CMs show identical FA size and number but different SF conformations. A-B) Representative fluorescent images of cFBs and hiPSC-CMs after 48 hours of static culture on homogeneous fibronectin coating, showing vinculin (green), actin SFs (magneta) and the cell nuclei (white). Scale bar indicates 25 µm. C-D) Schematic illustrations depicting the amount and distribution of FAs and SFs in cFBs and hiPSC-CMs. E-F) Quantification of FAs and SFs in both cell types indicates differences for the number of SFs per cell and the amount of active SFs (SFs/FAs). Results are expressed as mean ± SEM (n = 10 – 12 cells from 3 independent experiments).

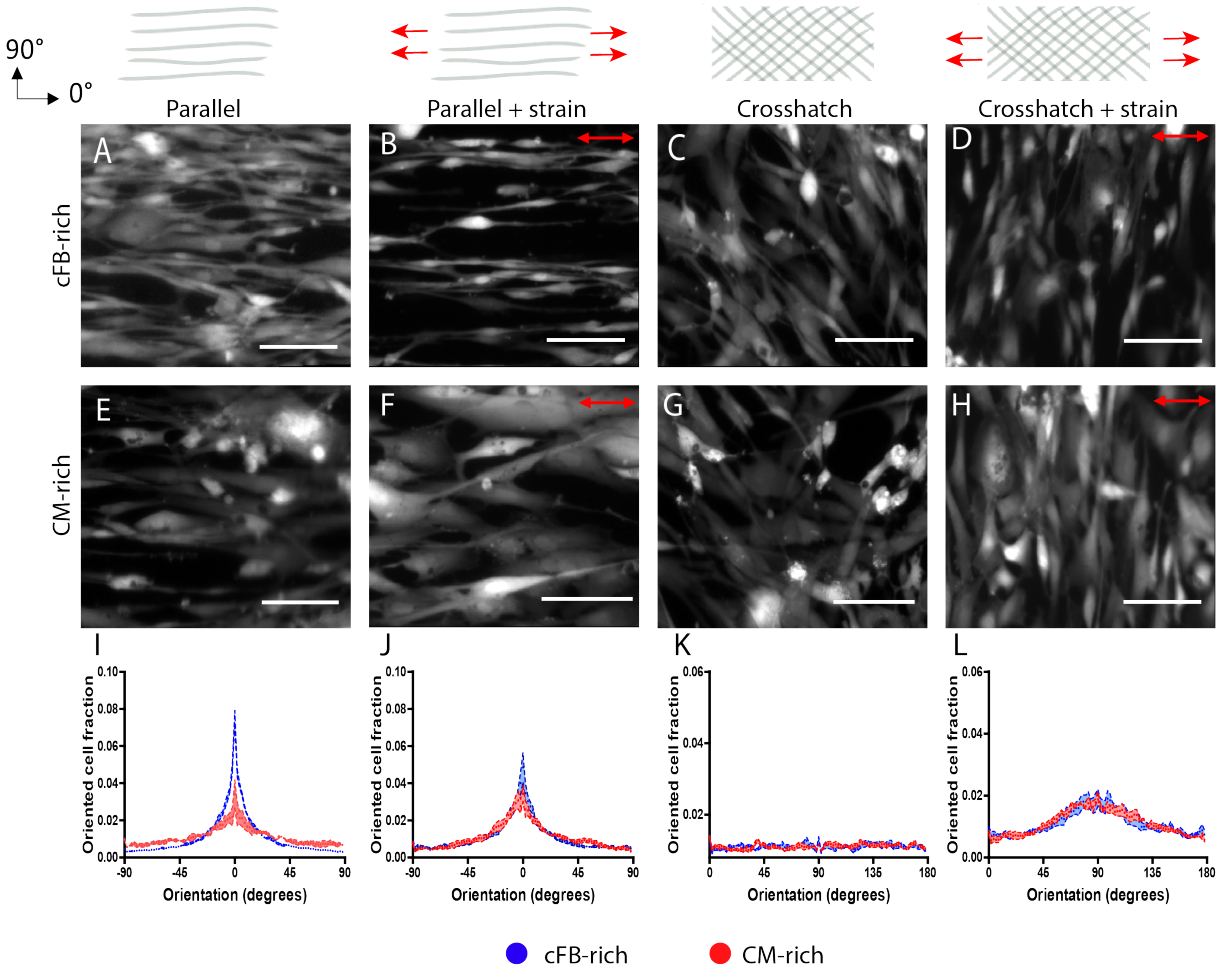

Figure 5: Pathology mimicking (cFB-rich) and normal (CM-rich) co-cultures show modest strain avoidance behavior in response to uniaxial cyclic strain A-H) Representative fluorescent images (calcein AM) of the co-cultures after 48 hours of dynamic culture on printed FN patterns. The direction of the uniaxial cyclic strain is depicted with the arrow. I-L) Frequency distributions that compare the response of cFB-rich co-cultures (blue) and CM-rich co-cultures (red) display the cell orientation corresponding to each co-culture. Scale bar indicates 100 µm. Results are expressed as mean ± SEM (n = 9 from 3 independent experiments).

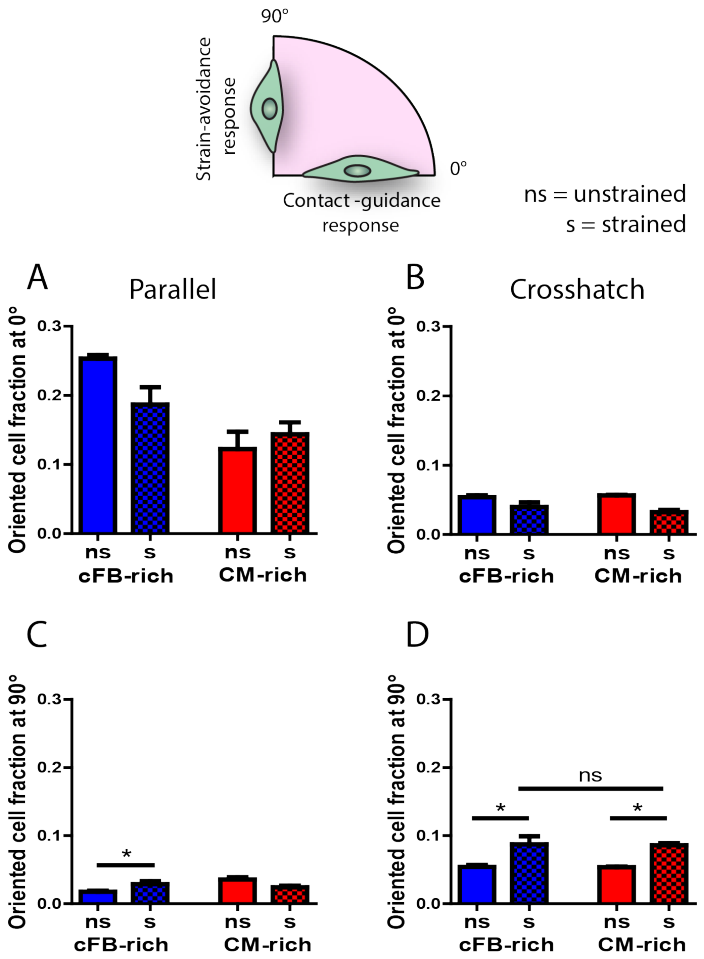

Figure 6: Uniaxial cyclic strain induces the alignment of both normal (CM-rich) and pathology mimicking (cFB-rich) co-cultures on crosshatch ECM. A - F) Oriented cell fractions at 0º ± 5º and 90º ± 5º show significant reorganization of the cFB-rich (blue) and CM-rich (red) co-cultures upon administration of uniaxial cyclic strain. Scale bar indicates 100 µm. Ns = non-strained, s = strained. Results are expressed as mean ± SEM (n = 9 from 3 independent experiments); * = P < 0.05; ** = P < 0.01.

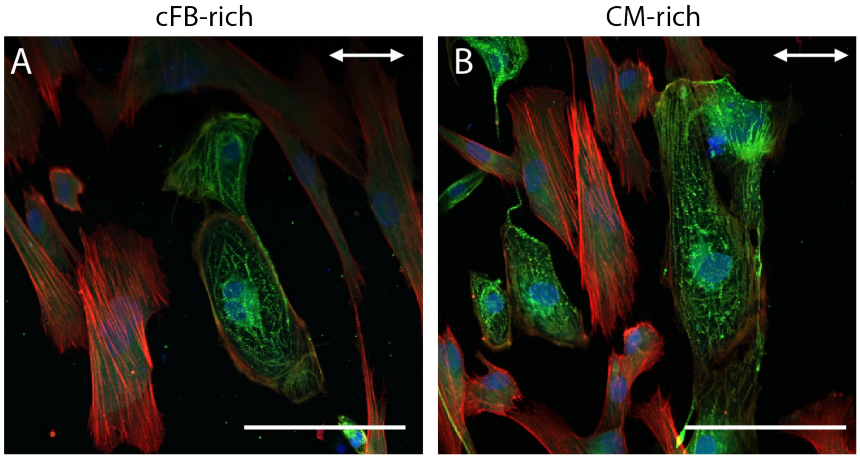

Figure 7: hiPSC-CMs and cFBs both show strain-avoidance in response to cyclic strain in cardiac co-cultures. A - B) Representative fluorescent images of cFBs and hiPSC-CMs after 48 hours of dynamic culture on crosshatch fibronectin coating, showing α-actinin (green, hiPSC-CMs), vimentin (red, cFBs) and the cell nuclei (white). Scale bar indicates 100 µm. The direction of the uniaxial cyclic strain is shown by the white arrow.